J. Phys.: Condens. Matter 7 (1995) 2489–2506. Printed in the UK

Optical properties of pyrochlore oxides $R_2Mo_2O_{7-\delta}$ (R: Sm, Gd, and Ho)

N Cao†, T Timusk†, N P Raju‡, J E Greedan‡ and P Gougeon§

† Department of Physics and Astronomy, McMaster University, Hamilton, Ontario, Canada L8S 4M1

‡ Department of Chemistry, McMaster University, Hamilton, Ontario, Canada L8S 4M1

§ Laboratoire Chimie du Solide et Inorganique Moleculaire, URA No 1495, Université de Rennes I—Beaulieu, 35042 Rennes, France

Received 25 October 1994, in final form 18 January 1995

Abstract. The temperature dependence of the reflectance of the spin glass materials $R_2Mo_2O_{7-\delta}$ (R: Sm, Gd, and Ho) has been measured for frequencies from 40 to 40 000 cm^{-1}. The AC conductivity of $Sm_2Mo_2O_{7-\delta}$, derived from Kramers–Kronig analysis, indicates a Drude-like behaviour as the temperature is lowered. Between 150 and 40 K the scattering rate shows a sharp drop which is attributed to the scattering of conduction electrons by short-range ordered moments of the Mo ions. Below the spin glass transition temperature T_f ($\simeq$40 K) the scattering rate saturates due to the freezing of the moments. $Gd_2Mo_2O_{7-\delta}$ behaves like a poor metal at room temperature, but at low temperatures shows a linear increase in the conductivity for frequencies up to 400 cm^{-1} suggesting a localized hopping conductivity. The localization remains in the spin glass state for $T < T_f$ ($\simeq$25 K). The conductivity of $Ho_2Mo_2O_{7-\delta}$ is semiconductor-like with a small and slightly temperature-dependent gap around 0.25 eV. Our optical results support a qualitative band model proposed by Sleight and Bouchard for the pyrochlore oxides.

1. Introduction

The pyrochlore oxides $R_2Mo_2O_{7-\delta}$ (R: one of the rare earth elements) show spin glass transitions at low temperatures, but they differ from usual spin glasses in the fact that the frustration results from *intrinsic geometrical* factors, rather than from a random distribution of magnetic or non-magnetic impurities [1, 2, 3, 4, 5]. One of the characteristic properties of a spin glass is a magnetic susceptibility that begins to deviate from the Curie law at temperatures $T \gg T_f$, where T_f is the spin freezing temperature. This property suggests that there are some short-range ordered moments present at higher temperatures. Also, in a metallic spin glass, the DC resistivity exhibits a broad maximum at a temperature $T_m \gg T_f$. This was found for example in AuCr, AuMn, AgMn, and CuMn alloys and was attributed to the scattering of conduction electrons by local magnetic clusters (short-range order) formed below T_m [6]. Reflectance spectroscopy can be used in a metallic $R_2Mo_2O_{7-\delta}$ material to study the temperature and, more importantly, the frequency dependence of the scattering rate of conduction electrons leading to information about the interaction between the conduction electrons and the magnetic Mo ions.

The DC resistivity of $R_2Mo_2O_{7-\delta}$ shows evidence of a metal–semiconductor transition as the size of the rare earth ion (R) is decreased [7]. Sleight and Bouchard (SB) have proposed a qualitative band model for pyrochlore oxides which is shown in figure 1 [8]. In this model,

0953-8984/95/122489+18$19.50

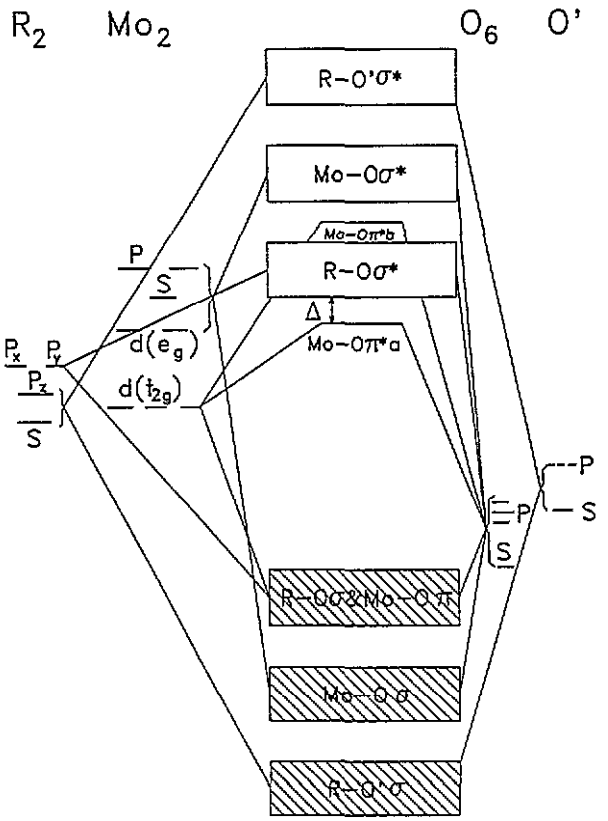

Figure 1. Band structure model of pyrochlore oxides proposed by Sleight and Bouchard (see [8]).

the transition is governed by the presence of a small gap between the full narrow Mo–O π^*a valence band and the empty broad R–O σ^* conduction band. Reflectance spectroscopy can be used to gain insight into electronic excitations in these materials. For non-metallic $R_2Mo_2O_{7-\delta}$ an absorption threshold should appear in the conductivity spectrum, if the absorption is due to electrons across the semiconducting gap. If the absorption is due to hopping within Anderson localized states, then a monotonically rising conductivity should appear in a low-frequency region at low temperatures [9]. No optical measurements exist for these materials, but with the recent availability of the $R_2Mo_2O_{7-\delta}$ single crystals (R: Sm, Gd, and Ho), the conduction mechanism in these materials can be investigated with optical techniques.

The crystal structure of the pyrochlore oxides has been determined by powder neutron and x-ray diffraction [10, 4]. These crystals have a face-centred cubic structure with a space group of $Fd\bar{3}m$. The R and Mo ions each form an infinite three-dimensional lattice of corner-sharing tetrahedra. With antiferromagnetic coupling between the nearest-neighbour Mo ions, such positions are highly frustrated.

The DC resistivity and susceptibility of the $R_2Mo_2O_{7-\delta}$ single crystals were measured using a four-probe technique and a SQUID magnetometer, respectively. The details of the results will be published separately [11]. Here we only show a brief result that is related to the optical results. Figure 2(a) shows the DC resistivity of a crystal of $Sm_2Mo_2O_{7-\delta}$. The resistivity increases slightly as the temperature is lowered from 300 to 150 K. As the

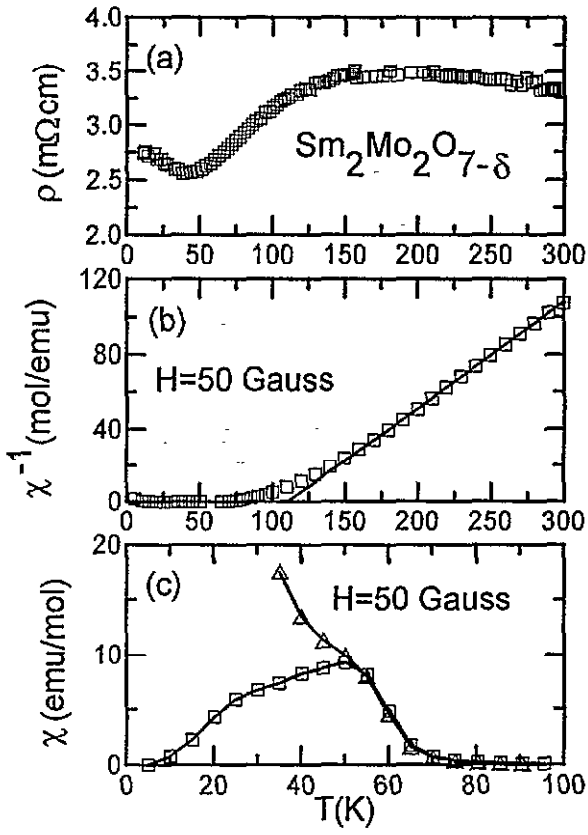

Figure 2. (a) The DC resistivity of $Sm_2Mo_2O_{7-\delta}$; (b) the inverse susceptibility of $Sm_2Mo_2O_{7-\delta}$ up to room temperature (the solid line is the result of the Curie law fitting at high temperatures); (c) the susceptibility of $Sm_2Mo_2O_{7-\delta}$ at low temperatures (squares: zero-field cooling data; triangles: field cooling data; solid lines: guide to the eye).

temperature is reduced further the resistivity drops sharply, but surprisingly, it turns up again at 40 K. The zero-field cooling (ZFC) inverse susceptibility, shown in figure 2(b), shows the Curie law behaviour at high temperatures and deviates from this law below ~150 K which is due to a partial short-range ordering of the Mo ion moments in this temperature range. From the Curie law fit, the Curie temperature Θ and effective moments p_{eff} were found to be 110 K and 2.6μ_B per $SmMoO_{3.5-\delta/2}$, respectively. Figure 2(c) shows the magnetic susceptibility of the $Sm_2Mo_2O_{7-\delta}$ crystal. Below the freezing temperature T_f (~50 K) the susceptibility depends on the history of the applied magnetic field: with ZFC some of the magnetic moments are frozen at low temperatures, a characteristic of spin glass materials.

The DC resistivity of the $Gd_2Mo_2O_{7-\delta}$ crystal, shown in figure 3(a), is quite different from that of $Sm_2Mo_2O_{7-\delta}$. The resistivity is non-metallic, increasing as temperature is lowered, but it also has a bump that appears between 10 and 35 K shown clearly in the inset. Figure 3(b) shows the inverse susceptibility of $Gd_2Mo_2O_{7-\delta}$. The deviation from the Curie law occurs around 100 K and from a fit to the higher-temperature data one obtains the values of Θ and p_{eff} of 25.9 K and 8.3μ_B per $GdMoO_{3.5-\delta/2}$, respectively. The susceptibility of the $Gd_2Mo_2O_{7-\delta}$ crystal shown in figure 3(c) is similar to that of $Sm_2Mo_2O_{7-\delta}$ and shows that some spins at the Mo ion sites are frozen below 25 K.

Figure 4(a) shows the DC resistivity of the $Ho_2Mo_2O_{7-\delta}$ crystal. It has an activated

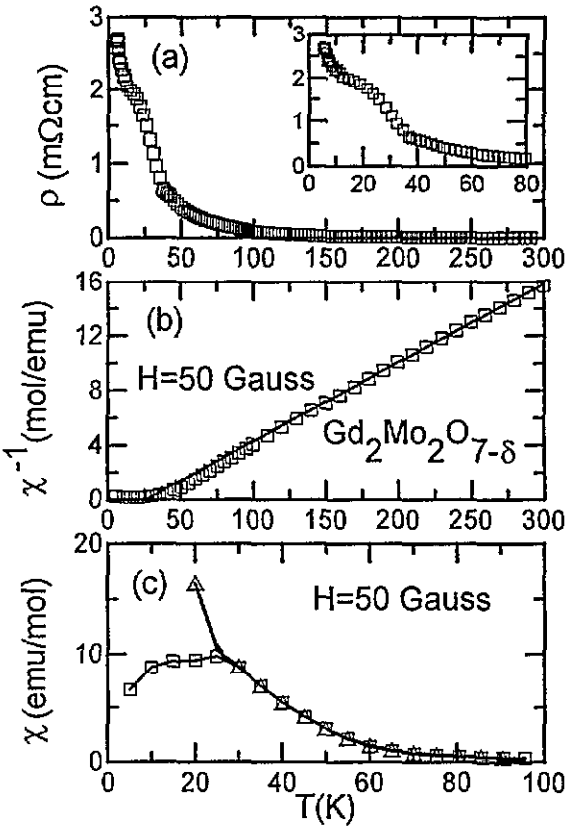

Figure 3. (a) The DC resistivity of $Gd_2Mo_2O_{7-\delta}$ up to room temperature. The inset is the DC resistivity at low temperatures. (b) The inverse susceptibility of $Gd_2Mo_2O_{7-\delta}$ up to room temperature. The solid line is the result of the Curie law fitting at high temperatures. (c) The susceptibility of $Gd_2Mo_2O_{7-\delta}$ at low temperatures (squares: zero-field cooling data; triangles: field cooling data; solid lines: guide to the eye).

semiconductive behaviour which is clearly shown in the inset of $\ln(\rho)$ against $1000/T$. The activation energy, E_a, deduced from the slope is 35 meV. The inverse susceptibility of the $Ho_2Mo_2O_{7-\delta}$ crystal up to room temperature is shown in figure 4(b). It adheres to the Curie law down to 20 K. The values of Θ and p_{eff} were found to be -1.3 K and 10.9 μ_B per $HoMoO_{3.5-\delta/2}$, respectively. Figure 4(c) shows the susceptibility of $Ho_2Mo_2O_{7-\delta}$ which suggests that a spin glass state develops below 20 K.

2. Experimental details

The optical measurements were performed on single crystals of $Sm_2Mo_2O_{7-\delta}$, $Gd_2Mo_2O_{7-\delta}$, and $Ho_2Mo_2O_{7-\delta}$. The crystals were glued to the tip of a pyramid-shaped sample holder which diffusely scatters all radiation that misses the sample. The sample and the stainless steel reference mirror were mounted on holders that were screwed onto the faces of a copper block cold finger and oriented at 90° with respect to each other. The cold finger was cooled using an R G Hansen High-Tran continuous-flow cryostat which could vary the sample temperature between 10 and 300 K. The temperature dependence of the reflectance was measured using a home-made Michelson interferometer for frequencies between 40

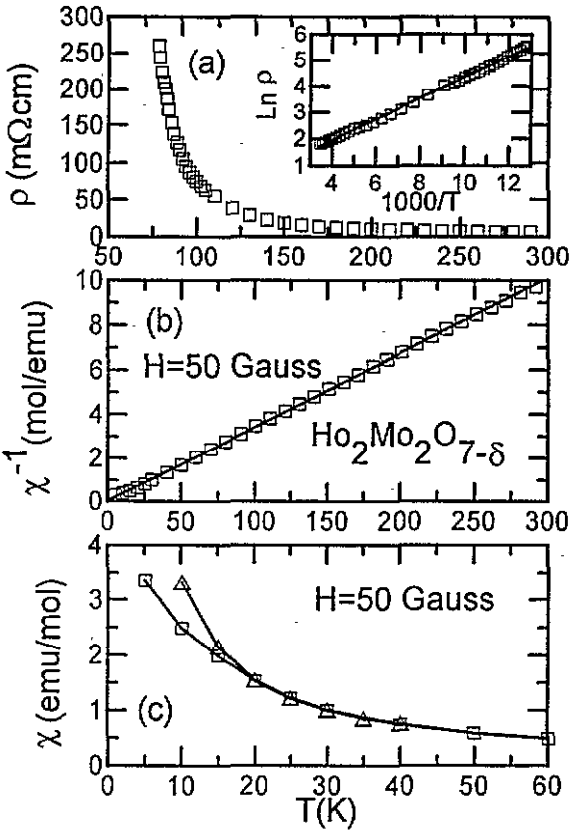

Figure 4. (a) The DC resistivity of $Ho_2Mo_2O_{7-\delta}$. The inset is the plot of $\ln(\rho)$ against $1000/T$. (b) The inverse susceptibility of $Ho_2Mo_2O_{7-\delta}$ up to room temperature. The solid line is the result of the Curie law fitting. (c) The susceptibility of $Ho_2Mo_2O_{7-\delta}$ at low temperatures (squares: zero-field cooling data; triangles: field cooling data; solid lines: guide to the eye).

and 9000 cm^{-1}. Another home-made grating spectrometer was used to measure the room-temperature reflectance from 3800 to 40 000 cm^{-1}. A normalized power spectrum was obtained by taking the ratio of the spectra from the sample and the reference mirror. At the end of the measurement a metallic film was evaporated *in situ* onto the sample surface. The geometrical differences between the sample and the reference mirror were taken into account by remeasuring the normalized power spectrum of the coated sample and the reference mirror at each temperature. The absolute value of the reflectance of the sample was obtained by taking a ratio of these two normalized power spectra and multiplying the ratio with the known reflectance of the evaporated metal [12].

3. Results and discussion

3.1. $Sm_2Mo_2O_{7-\delta}$

Figure 5 shows the far-infrared reflectance spectra of $Sm_2Mo_2O_{7-\delta}$ at five temperatures. All spectra have phonon peaks superimposed on a background showing a characteristic metallic decrease of reflectance with frequency. As temperature is reduced the reflectance increases uniformly for all but the 10 K data. Its reflectance is higher than the 40 K data

only for frequencies below 150 cm^{-1}. The inset to figure 5 shows the room-temperature reflectance of $Sm_2Mo_2O_{7-\delta}$ up to 40 000 cm^{-1}. It decreases smoothly with frequency up to 10 000 cm^{-1}, followed by an increase due to the presence of a broad peak centred at 30 000 cm^{-1}. Low- and high-frequency extrapolations of the reflectance data must be used in the calculation of the optical constants using Kramers–Kronig analysis. At low frequencies the relation $R = 1 - A\sqrt{\omega}$ was used to extrapolate the reflectance, where A is a constant determined by the value of the reflectance at the lowest experimental frequency. The room-temperature reflectance between 700 and 40 000 cm^{-1} was used to extend the low-temperature reflectance spectra. This extrapolation does not significantly alter the low-frequency conductivity since the slopes of the low-temperature spectra are similar to that of the room-temperature data. Beyond 40 000 cm^{-1} the reflectance was extrapolated using an ω^{-4} frequency dependence.

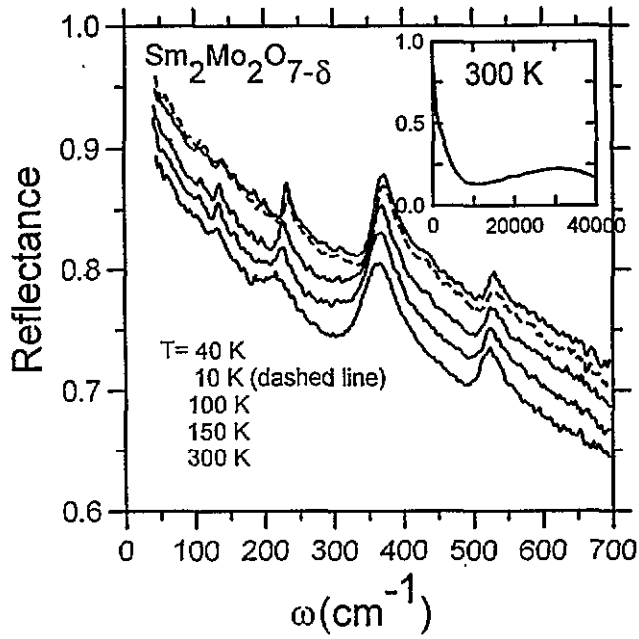

Figure 5. Reflectance of $Sm_2Mo_2O_{7-\delta}$ at far-infrared frequencies at 10 (dashed line), 40, 100, 150, and 300 K (from top to bottom). The inset shows the reflectance of $Sm_2Mo_2O_{7-\delta}$ up to 40 000 cm^{-1} at 300 K.

The inset to figure 6 shows the room-temperature optical conductivity of $Sm_2Mo_2O_{7-\delta}$ obtained from Kramers–Kronig analysis. Note that there is a broad absorption peak centred at 25 000 cm^{-1} which is associated with the reflectance peak around 30 000 cm^{-1}. It is assigned as an interband transition between the lower valence band and the conduction band. This will be discussed in more detail later on.

The conductivity of $Sm_2Mo_2O_{7-\delta}$ at far-infrared frequencies is shown in figure 6. The overall conductivity consists of two components: (1) the sharp phonon absorption peaks and (2) the continuum background. To isolate the continuum background in $\sigma_1(\omega)$ the phonon lines were fitted to Fano lineshapes [13] with the baseline fitted to constant, linear, and quadratic terms as shown in the following formula:

$$\sigma_1(\omega) = a + b\omega + c\omega^2 + \sum_{i=1}^{n} d_i \frac{x_i + q_i}{1 + x_i^2} \tag{1}$$

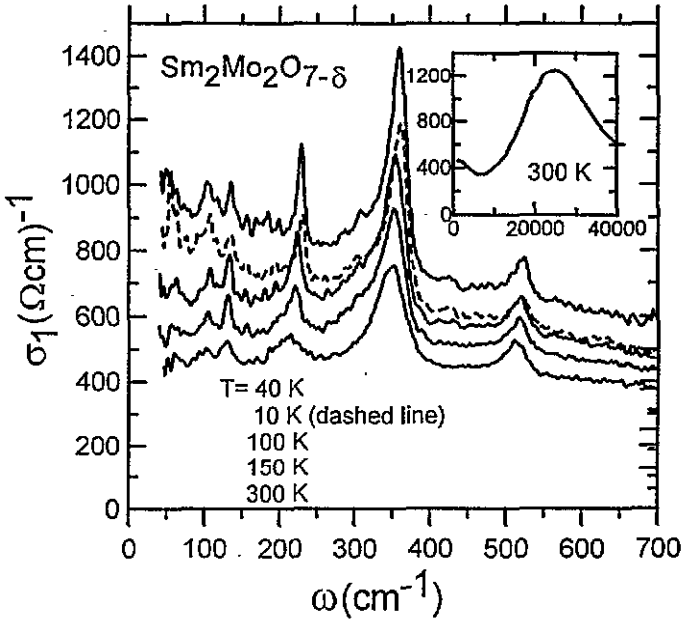

Figure 6. Real part of the far-infrared AC conductivity of $Sm_2Mo_2O_{7-\delta}$ at 10 (dashed line), 40, 100, 150, and 300 K (from top to bottom). The inset shows the real part of the AC conductivity of $Sm_2Mo_2O_{7-\delta}$ at 300 K as a function of frequency up to 40 000 cm^{-1}.

where $x_i = (\omega - \omega_i)/\gamma_i$, a, b, and c are constants, n is the total number of the phonon lines, ω_i is the phonon frequency, γ_i and d_i are width and strength parameters, respectively, and q_i describes the asymmetry of the ith phonon. Note that the Fano lineshape will be symmetric if $q_i \gg x_i$†. There are six phonon modes in $\sigma_1(\omega)$ (the lowest-frequency mode in the 100, 150, and 300 K data is very weak). All modes except the one at 345 cm^{-1} are symmetric. Little temperature dependence was found in the 101, 129, and 510 cm^{-1} modes. The 210 cm^{-1} mode narrows and hardens at low temperatures. The 345 cm^{-1} mode is symmetric at room temperature. At lower temperatures it becomes asymmetric (i.e. the absolute value of q decreases) and hardens.

The phonon fits were used to subtract their contribution from the total conductivity, leaving only the background conductivity $\sigma_1^b(\omega)$ shown in figure 7. The DC conductivity of the $Sm_2Mo_2O_{7-\delta}$ crystal at 300 K is shown as a filled square on the left vertical axis. There is a nearly 150 Ω^{-1} cm^{-1} difference between the DC conductivity and the extrapolated value. Note that $\sigma_1^b(\omega)$ at room temperature decreases only slightly with increasing frequency. This is characteristic of a poor metal with a broad Drude peak centred at zero frequency. As the temperature is lowered $\sigma_1^b(\omega)$ increases in a Drude-like manner. A conductivity anomaly occurs in the 10 K data where $\sigma_1^b(\omega)$ shifts *downward* in comparison to the 40 K data. This unusual behaviour is in accord with the DC resistivity of $Sm_2Mo_2O_{7-\delta}$ which shows a resistive minimum at 40 K. The Drude model,

$$\sigma_D(\omega, T) = \frac{\omega_p(T)^2 \gamma_D(T)}{4\pi[\omega^2 + \gamma_D(T)^2]} \tag{2}$$

where $\gamma_D(T)$ and $\omega_p(T)$ are the scattering rate and plasma frequency, respectively, was used

† All of the fitting parameters of the Fano lineshapes for $R_2Mo_2O_{7-\delta}$ (R: Sm, Gd, and Ho) are available to interested readers upon request and the e-mail address is: caon@mcmail.cis.mcmaster.ca.

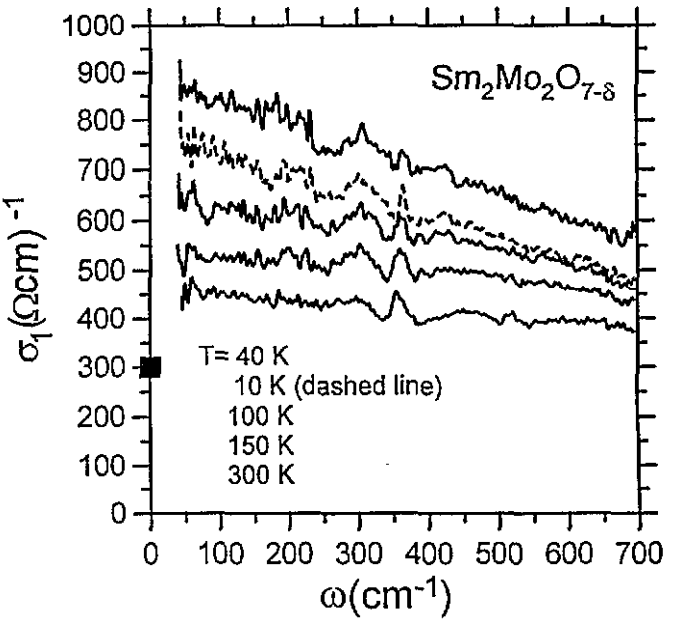

Figure 7. Background AC conductivity of $Sm_2Mo_2O_{7-\delta}$ obtained by subtracting the phonon absorption peaks from the overall conductivity at each temperature. The value of the DC conductivity of $Sm_2Mo_2O_{7-\delta}$ at 300 K is shown as a filled square on the left vertical axis.

to fit the background conductivity. Figure 8 shows the resulting temperature dependence of these two parameters. The scattering rate gently decreases as the temperature is lowered from 300 to 150 K. At lower temperatures it drops sharply until it finally saturates for temperatures below 40 K. Above 150 K the slope of $\gamma_D(T)$ results from phonons and one gets $\lambda = 0.19$ using the formula $\gamma_D(T) = 2\pi\lambda k_B T$, where λ is the electron–phonon coupling constant. The scattering of conduction electrons from the short-range ordered Mo ions, which sets in at about 150 K, causes the sharp decrease of $\gamma_D(T)$ between 150 and 40 K. The fact that in the temperature range of 40 to 150 K the behaviour of $\gamma_D(T)$ is similar to that of the DC resistivity of $Sm_2Mo_2O_{7-\delta}$ implies that the sharp decrease in the scattering rate gives rise to the steep drop in the DC resistivity. If this picture is correct, the saturation of $\gamma_D(T)$ below 40 K is due to the freezing of moments on the Mo ions.

It is noted that the overall scattering rate of $Sm_2Mo_2O_{7-\delta}$ is quite large, much larger than what is seen in conventional metals, but it is comparable with that of other magnetic systems such as chromium ($\gamma_D(T = 300\ K) \simeq 340\ cm^{-1}$), URu_2Si_2 ($\gamma_D(T = 90\ K) \simeq 3000\ cm^{-1}$) and UNi_2Si_2 ($\gamma_D(T) \simeq 500\ cm^{-1}$ at 140 K in the basal plane and 800 cm^{-1} at 300 K along the c-axis) [14, 15, 16]. Also note that the overall scattering rate of $Sm_2Mo_2O_{7-\delta}$ consists of two components: the temperature-dependent one, which has been discussed before, having phonon and magnetic origins, and the temperature-independent background which is associated with the large temperature-independent component of the DC resistivity of $Sm_2Mo_2O_{7-\delta}$. The origin of this background is not clear, however, the fact that there is always some large temperature-independent component in the DC resistivity of conventional metallic spin glass materials suggests that it might be related to impurity scattering [6].

The Drude plasma frequency $\omega_p(T)$ increases slightly as the temperature is lowered from 300 to 150 K. It then drops from 150 to 70 K and another maximum appears at 40 K. Finally, it drops again from 40 to 10 K. The decrease of $\omega_p(T)$ from 40 to 10 K gives rise to an

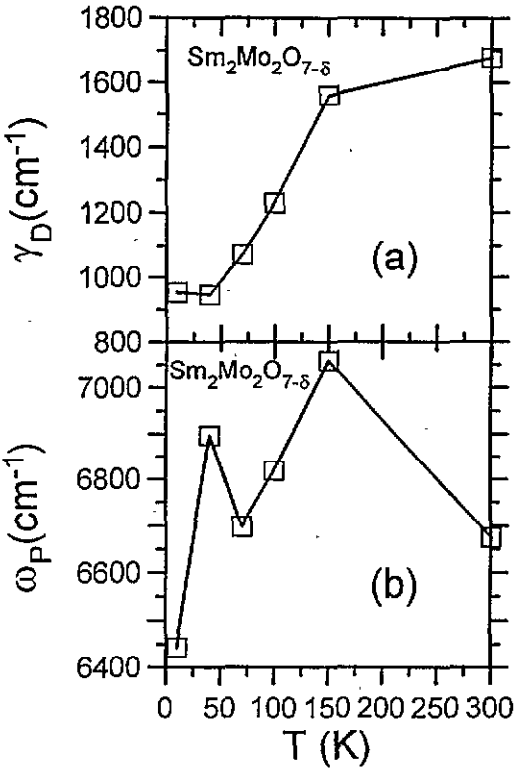

Figure 8. (a) The temperature dependence of the scattering rate of $Sm_2Mo_2O_{7-\delta}$ found by fitting the background conductivity in figure 7 to the Drude conductivity formula; (b) the temperature dependence of the plasma frequency of $Sm_2Mo_2O_{7-\delta}$.

increase in the DC resistivity and a decrease in the AC conductivity in the same temperature range. The slight increase in the DC resistivity from 300 to 150 K cannot be explained by the optical results, which suggest that the resistivity *decreases* in this temperature range. It should be noted that a room-temperature carrier density of 5.0×10^{20} cm^{-3} is obtained from the plasma frequency, assuming that the effective mass of the conduction electrons is equal to that of the free electron. This value is characteristic of a poor metal.

The behaviour of $\gamma_D(T)$, which mainly has a magnetic origin, can be understood in terms of a picture of the temperature dependence of the spin correlation function $\langle S(0)S(r)\rangle$ of the Mo ions, where r is the spacing between two nearest-neighbour Mo ions. The correlation function is quite small at high temperatures due to thermal fluctuations, begins to increase as the temperature is reduced to the value of the exchange integral, J, which is proportional to the Curie temperature Θ (= 110 K), and saturates as spins on the Mo ion sites are frozen below T_f. Therefore, the scattering experienced by conduction electrons from the magnetic Mo ions is incoherent at high temperatures, becomes more and more coherent as the correlation develops, and, finally, reaches a constant value as a result of the saturation of the spin correlation.

At this stage it is unclear why the DC resistivity of $Sm_2Mo_2O_{7-\delta}$ shows the upturn below 40 K. One possibility could be a pseudogap opened at the Fermi surface with an energy scale below our experimental limit. The decrease in the plasma frequency in this temperature region might mean a reduction in the free carrier density provided that the effective mass of free carriers is constant. It is also possible that the upturn is due to the Kondo effect with spin exchanges between Sm ions and conduction electrons. It is an open question whether or not there is a physical connection between the DC resistivity anomaly and the

spin frustrations in the spin glass state.

3.2. $Gd_2Mo_2O_{7-\delta}$

The temperature-dependent far-infrared reflectance of $Gd_2Mo_2O_{7-\delta}$ is shown in figure 9. The room-temperature spectrum is similar to that of $Sm_2Mo_2O_{7-\delta}$, in that there are some phonon peaks superimposed on a background reflectance that decreases with frequency. In contrast to $Sm_2Mo_2O_{7-\delta}$ the overall reflectance of $Gd_2Mo_2O_{7-\delta}$ decreases as the temperature is lowered. However, this result is consistent with the DC resistivity measurement which shows an increasing resistivity as the temperature is lowered. Note that an anomaly occurs in the 25 K data. When comparing it to either the 10 K or 100 K data it is apparent that the reflectance is higher at low frequencies and lower at high frequencies. The inset to figure 9 shows the room-temperature reflectance of $Gd_2Mo_2O_{7-\delta}$ up to 40 000 cm^{-1}. The reflectance decreases with frequency up to 10 000 cm^{-1} where it turns up and has a peak centred at 35 000 cm^{-1}. The extrapolations used for Kramers–Kronig analysis were the same as those used for $Sm_2Mo_2O_{7-\delta}$. The resulting room-temperature conductivity up to 35 000 cm^{-1} is shown in the inset to figure 10. As was the case with $Sm_2Mo_2O_{7-\delta}$ there exists a strong interband transition peak centred near 27 500 cm^{-1}.

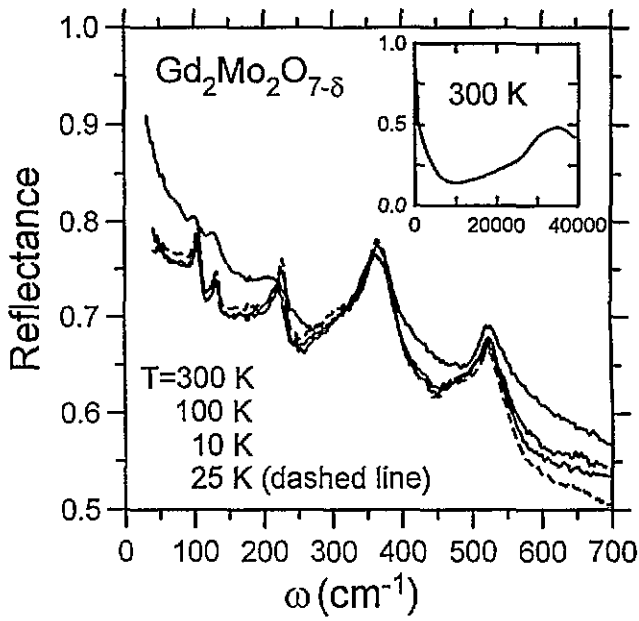

Figure 9. Reflectance of $Gd_2Mo_2O_{7-\delta}$ in the far-infrared region at 300, 100, 25 (dashed line), and 10 K (from top to bottom). The inset shows the reflectance of $Gd_2Mo_2O_{7-\delta}$ at 300 K up to 40 000 cm^{-1}.

Figure 10 shows the temperature-dependent far-infrared optical conductivity of $Gd_2Mo_2O_{7-\delta}$. Excluding the 25 K data, it consists of phonon peaks superimposed on a continuum background which decreases in strength as the temperature is reduced. This behaviour is different from that of $Sm_2Mo_2O_{7-\delta}$ at low temperatures. As was the case for $Sm_2Mo_2O_{7-\delta}$ equation (1) was used to fit $\sigma_1(\omega)$ allowing a separation of the phonon and background contributions to the conductivity.

The background conductivity $\sigma_1^b(\omega)$ of $Gd_2Mo_2O_{7-\delta}$ at 300, 100, 25, and 10 K is shown

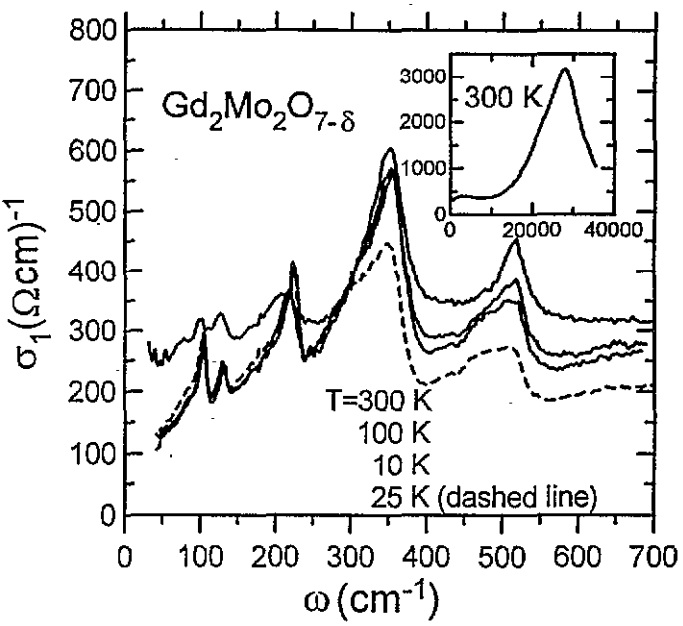

Figure 10. Real part of the far-infrared AC conductivity of $Gd_2Mo_2O_{7-\delta}$ as a function of frequency at 300, 100, 25 (dashed line), and 10 K (from top to bottom). The inset shows the real part of the AC conductivity of $Gd_2Mo_2O_{7-\delta}$ at 300 K as a function of frequency up to 35 000 cm^{-1}.

in figure 11. Also shown is the DC conductivity of $Gd_2Mo_2O_{7-\delta}$ at 100 and 300 K. Note that the room-temperature DC conductivity is nearly 100 Ω^{-1} cm^{-1} smaller than the extrapolated value at zero frequency. Also note that the room-temperature conductivity increases slightly with frequency. At low temperatures a conductivity depression occurs below 400 cm^{-1}.

The conductivity behaviour of $Gd_2Mo_2O_{7-\delta}$ can be understood in terms of Anderson localization. In this model the Fermi level E_F is in the region of the density of states where the states are localized and DC conductivity is induced by excitations of conduction electrons to the mobility edge E_c, which separates localized states from extended states. The almost frequency-independent AC conductivity at room temperature is due to optical excitations of those electrons which have been thermally activated to E_c and, therefore, behaves like a poor metal. The hopping conductivity has been studied by Mott and Davis. They have given an expression describing the temperature and frequency dependence of $\sigma_1(\omega)$ [17]. The linear-dependent conductivity with frequency up to 400 cm^{-1} displayed by $Gd_2Mo_2O_{7-\delta}$ at 100, 25, and 10 K is in agreement with the theory of Mott and Davis and is due to the optically activated hopping of conduction electrons within localized states. It should be pointed out that such a hopping conduction process has been found in the far-infrared absorption spectrum of the neutron-transmutation-doped germanium [18].

Mott pointed out that for Anderson localization the DC conductivity behaves as $\simeq \sigma_0 \exp[-(E_c - E_F)/k_B T]$ at high temperatures and $\simeq \sigma_1 \exp[-(Q/k_B T)^{0.25}]$ (the variable-range hopping conductivity) at sufficiently low temperatures, where $Q = 1.5\alpha^3/N(E_F)$, $N(E_F)$ is the density of states at E_F and α represents the fall-off rate of the envelope of the wave function $\phi \sim \exp(-\alpha r)$ [19]. This behaviour has been observed in the $(Dy_xY_{1-x})_2Mo_2O_7$ pyrochlore materials by Raju and Rangarajan [20]. The following

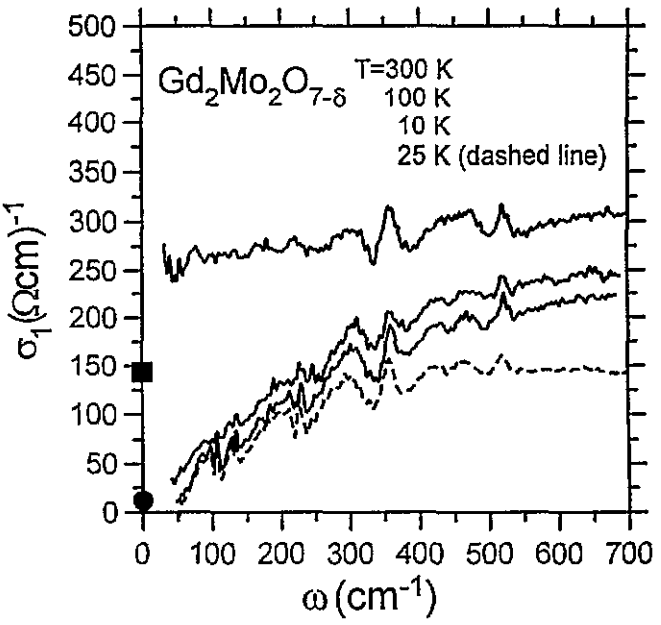

Figure 11. Background AC conductivity of $Gd_2Mo_2O_{7-\delta}$ which was obtained by subtracting the phonon peaks from the overall conductivity shown in figure 10 at 300, 100, 25 (dashed line), and 10 K (from top to bottom). The values of the DC conductivity of $Gd_2Mo_2O_{7-\delta}$ at 300 and 100 K are shown on the left vertical axis as a filled square and circle, respectively.

formula,

$$\sigma = \sigma_0 \exp[-(E_c - E_F)/k_B T] + \sigma_1 \exp[-(Q/k_B T)^{0.25}] \tag{3}$$

was used to fit the DC conductivity of $Gd_2Mo_2O_{7-\delta}$. Figure 12 shows the result of the fit together with the DC conductivity data. The fit is good at high and very low temperatures ($T \leqslant 25$ K), but it does not agree with the experimental data at intermediate temperatures. The resulting parameters are $\sigma_0 = 678\ \Omega^{-1}\ cm^{-1}$, $E_c - E_F = 324\ cm^{-1}$, $\sigma_1 = 1.81\ \Omega^{-1}\ cm^{-1}$, and $Q = 1.70\ cm^{-1}$. Le Comber *et al* studied the transport properties of amorphous Si films [21]. In their studies the temperature dependence of the DC conductivity was divided into three regions: from room temperature to the temperature T_1 the conductivity is due to thermal excitations of carriers to the mobility edge with an activation energy $E_c - E_F$; the slope of $\ln[\sigma_{DC}(T)]$ against $1/T$ changes at T_1. Between T_1 and T_2 the conductivity takes place through phonon-assisted hopping within the localized states and is still activated but with a smaller energy $E_x - E_F + W_e$, where E_x is the energy around which hopping occurs and W_e is the hopping energy; for $T < T_2$, E_x approaches E_F and W_e decreases as the temperature is lowered. As E_x approaches E_F the conductivity is $\propto \exp[(-Q/k_B T)^{0.25}]$.

The DC conductivity of $Gd_2Mo_2O_{7-\delta}$ can also be divided into three regions: the high-temperature region between room temperature and T_1 ($\simeq$180 K), in which $E_c - E_F = 324\ cm^{-1}$, the intermediate-temperature region between T_1 and T_2 ($\simeq$25 K) where the slope of $\ln[\sigma_{DC}(T)]$ against $1/T$ decreases continuously, and the low-temperature region for $T < T_2$ where the conductivity is described by variable-range hopping. The difference between $Gd_2Mo_2O_{7-\delta}$ and amorphous Si film is that the slope is not constant for $Gd_2Mo_2O_{7-\delta}$ in the intermediate-temperature region which indicates that the movement of E_x towards E_F and the drop of W_e have already taken place in this region. This could be caused by a

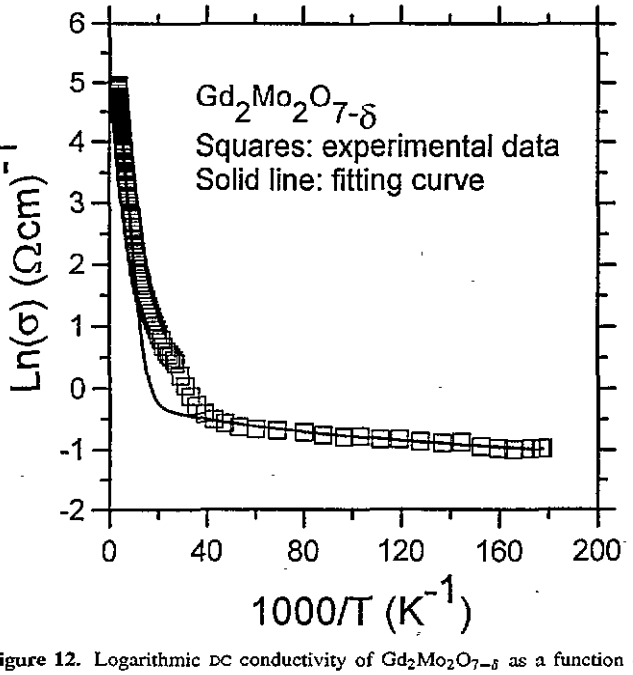

Figure 12. Logarithmic DC conductivity of $Gd_2Mo_2O_{7-\delta}$ as a function of $1000/T$ shown as squares. The solid line is the fitted result using equation (3) in the text.

magnetic interaction between conduction electrons and magnetically short-range ordered Mo ions. Our far-infrared optical results shown in figure 11 support this interpretation. The almost flat AC conductivity at 300 K results from optical excitations of conduction electrons in the extended states just above E_c, whereas at low temperatures the conductivity begins to be depressed at 400 cm^{-1}, which is roughly equal to the value of $E_c - E_F$ given above, and this is caused by the optically activated hopping of electrons in the localized states below E_c. Using the fitted Q and assuming $\alpha^{-1} = 10$ Å, the same order as the lattice constant a ($\simeq$10 Å), then one gets $N(E_F) \simeq 4 \times 10^{23}$ cm^{-3} eV^{-1}, a reasonable value slightly higher than that of a typical semimetal.

It should be noted that there is a conductivity anomaly in the 25 K data: $\sigma_1^b(\omega)$ at this temperature is lower than that at 10 K. As mentioned earlier there is a bump in the DC resistivity between 10 and 35 K. Also, a Curie temperature of 26 K is deduced from fitting the high-temperature susceptibility. These two observations suggest that there might be another scattering process around 25 K which has a magnetic origin. We believe that this extra scattering is responsible for the presence of the AC conductivity anomaly at 25 K and may be caused by spin frustrations which exist in the spin glass state around 25 K.

At room temperature $Gd_2Mo_2O_{7-\delta}$ has five symmetric phonon modes at 99, 126, 204, 345, and 512 cm^{-1}. As the temperature is reduced the phonon line shapes become asymmetric which is quantified by the dramatic reduction in the absolute value of the parameter q (the only exception is the 126 cm^{-1} mode at 10 and 25 K). The 99, 126, and 204 cm^{-1} modes narrow and the 10 K data show that the mode positions shift to 104, 131, and 225 cm^{-1}, respectively. The width of the 345 cm^{-1} mode does not change as the temperature is reduced to 10 K, but it does shift to 360 cm^{-1}. The 512 cm^{-1} mode becomes broader and hardens to 520 cm^{-1}. In Fano's paper the width of the resonance, 2γ, is equal to $2\pi|V_E|^2$, where V_E is the coefficient of the resonance–continuum (in our case the

electron–phonon, e–p) interaction and the position of resonance is at $E = E_\varphi + F$, where E_φ is the position with $V_E = 0$ and $F(E) = P\int dE' |V_{E'}|^2/(E - E')$ which determines the shift of the position of the resonance [13]. The localization of the free carriers at low temperatures causes a reduction of e–p interaction and gives rise to the narrowing of the three lowest-frequency modes. The increase of the e–p interaction for the 512 cm^{-1} mode at low temperatures leads to the widening of this mode. These two effects cancel each other out for the 345 cm^{-1} mode because at this frequency most of the electrons at localized states are excited to the extended states above E_c. This accounts for its unchanged width. The shape of the phonons can be understood qualitatively. According to Fano's paper [13]

$$q = \frac{(\Phi|T|i)}{\pi V_E'(\psi_E|T|i)} \tag{4}$$

where $(\Phi|T|i)$ is the transition matrix element between an initial state i and the modified discrete state Φ, in which a real discrete state φ is admixed with states of the continuum, and $(\psi_E|T|i)$ is another transition matrix element between the state i and the unperturbed continuum state ψ_E. We assume that the numerator in equation (4) is a dominant factor in determining the value of q. At low temperatures electrons are localized and the conductivity results from phonon-assisted hopping so that the matrix element $(\Phi|T|i)$ is much smaller, and, therefore, q is much smaller causing the phonon shape to be asymmetric. At room temperature conduction electrons in the extended region can be optically excited to a higher energy level without phonon assistance and as a result $(\Phi|T|i)$ becomes larger which leads to a symmetric phonon shape.

3.3. $Ho_2Mo_2O_{7-\delta}$

The frequency dependence of the reflectance of $Ho_2Mo_2O_{7-\delta}$ at 300, 100, 40, and 10 K is shown in Figure 13. At far-infrared frequencies several phonons are superimposed on a smooth background reflectance that decreases with increasing frequency at each temperature. The overall reflectance decreases between 300 and 100 K and becomes temperature independent below 100 K. Unlike the $Sm_2Mo_2O_{7-\delta}$ and $Gd_2Mo_2O_{7-\delta}$ reflectance spectra, the $Ho_2Mo_2O_{7-\delta}$ spectrum shows a sharp drop at the end of the far-infrared region with a minimum at 700 cm^{-1}. This feature is independent of temperature and develops into a deep valley at low temperatures. Interestingly, a peak shows up near 2000 cm^{-1} which is absent from the reflectance spectra of $Sm_2Mo_2O_{7-\delta}$ and $Gd_2Mo_2O_{7-\delta}$ and changes slightly as the temperature is lowered. The inset to figure 13 shows the room-temperature reflectance spectrum up to 40 000 cm^{-1}. It exhibits a broad peak at high frequencies.

The temperature dependence of the optical conductivity of $Ho_2Mo_2O_{7-\delta}$, obtained from the Kramers–Kronig transformation using the same extrapolations as before, is displayed in figure 14(a). In the far-infrared region, three phonons can be seen superimposed on a continuous background. The background becomes weaker as the temperature is lowered from 300 to 100 K and is independent of temperature below 100 K. The background conductivity is separated from phonons using the same procedure as the one used for $Sm_2Mo_2O_{7-\delta}$ and $Gd_2Mo_2O_{7-\delta}$. All phonon modes except the one at 225 cm^{-1} are symmetric. As the temperature is reduced, all modes harden with little change in their widths. The inset to figure 14(a) shows the resulting far-infrared background conductivity at 300 and 100 K. It is essentially independent of frequency and the magnitude changes from 70 (Ω^{-1} cm^{-1}) at 300 K to 20 (Ω^{-1} cm^{-1}) at 100 K. The value of the DC conductivity at 300 K is 163 Ω^{-1} cm^{-1} which is 90 Ω^{-1} cm^{-1} larger than the value of the far-infrared conductivity extrapolated to zero frequency at the same temperature. It is reminiscent of the

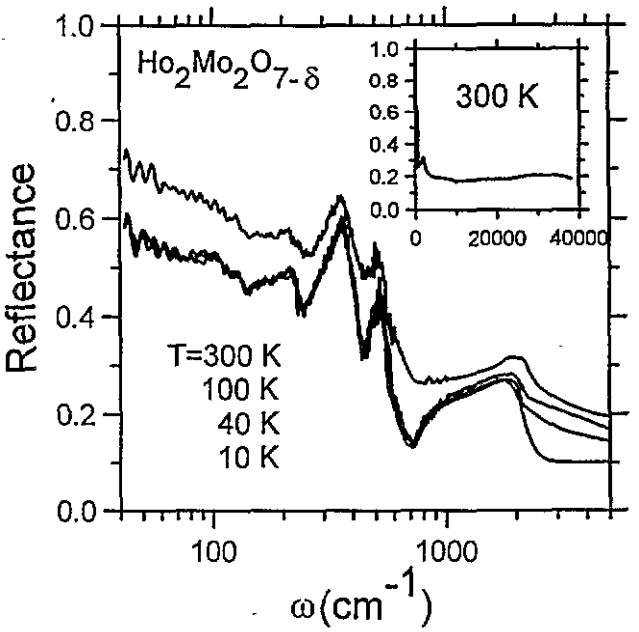

Figure 13. Reflectance of $Ho_2Mo_2O_{7-\delta}$ in the frequency range up to 5000 cm^{-1} at 300, 100, 40, and 10 K (from top to bottom). The inset shows the reflectance of $Ho_2Mo_2O_{7-\delta}$ at 300 K up to 40 000 cm^{-1}.

free carrier conductivity of a semiconductor which decreases as the temperature is lowered. There are several problems with this idea. Firstly, the flatness of the conductivity implies a very large scattering rate, of the order of the bandgap. Secondly, it is hard to understand the temperature-independent conductivity below 100 K. It seems that the conductivity somehow reaches a minimum value at 100 K and cannot decrease further. It should be noted that an asymmetric peak appears around 2000 cm^{-1}. This peak shifts slightly towards lower frequencies with decreasing temperature and does not change below 40 K. There is no interband transition around 2000 cm^{-1} due to the crystal field effect of Ho^{3+} [22]. It appears to be due to excitations of electrons across a small semiconducting gap Δ with a value $\simeq$2000 cm^{-1} ($\sim$0.25 eV) between the valence band (next to the conduction band) and the conduction band. This will be discussed in detail in the next subsection. Figure 14(b) shows the room-temperature conductivity spectrum over a wider range, up to 40 000 cm^{-1}. Generally, the conductivity increases with frequency and there is a broad interband transition peak centred at 32 000 cm^{-1} which has also been seen in $Sm_2Mo_2O_{7-\delta}$ and $Gd_2Mo_2O_{7-\delta}$ at the two different frequencies. Note that there is a weak structure around 10 000 cm^{-1} which is not real. It is due to a small structure in the merge area of the reflectance spectra from two runs of the experiment covering two different frequency ranges, shown in the inset to figure 13 around 10 000 cm^{-1}.

3.4. Discussion

According to the SB model the band structure of pyrochlore oxides, which is shown schematically in figure 1, can be considered in terms of two interpenetrating networks of R_2O and $2MoO_3$ [8]. The two hybridization bands, the (full) narrow Mo–O π^*a valence band and the (empty) broad R–O σ^* conduction band, are separated by a small

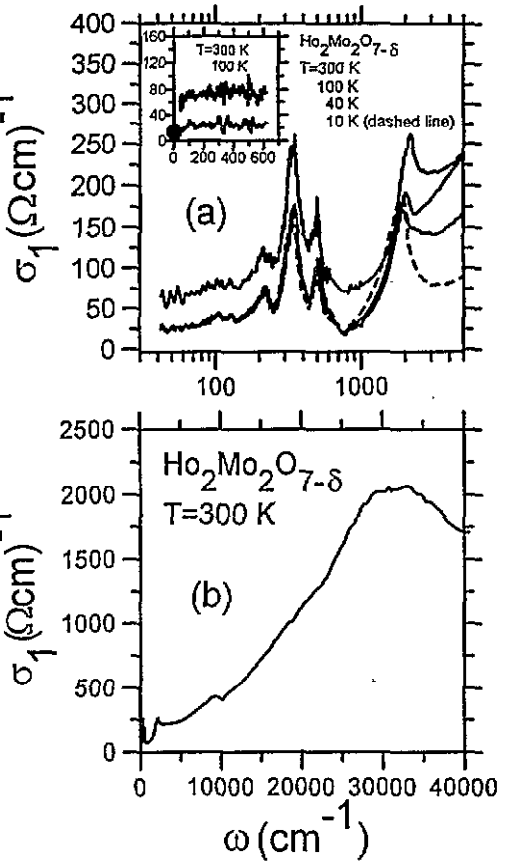

Figure 14. (a) The real part of the AC conductivity of $Ho_2Mo_2O_{7-\delta}$ as a function of frequency at 300, 100, 40, and 10 (dashed line) K (from top to bottom). The inset shows the far-infrared background conductivity at 300 and 100 K (top and bottom). The value of the DC conductivity of $Ho_2Mo_2O_{7-\delta}$ at 100 K is shown on the left vertical axis as a filled circle. (b) The real part of the AC conductivity of $Ho_2Mo_2O_{7-\delta}$ at 300 K as a function of frequency up to 40 000 cm^{-1}.

energy gap Δ in the semiconducting $R_2Mo_2O_{7-\delta}$ materials with a smaller ionic radius of R^{3+}. As the radius increases the conduction band moves downward and these two bands ultimately overlap leading to the metallic behaviour. The big absorption peak observed in the optical conductivity spectra of $R_2Mo_2O_{7-\delta}$ at high frequencies can be assigned to optical excitations of electrons across the interband gap E_g between the lower filled R–O σ and Mo–O π valence band and the conduction band. Figure 15 shows the interband gap E_g of $R_2Mo_2O_{7-\delta}$ as a function of the ionic radius of R^{3+}. It was found that E_g increases linearly with decreasing ionic radius which attests to the applicability of the SB model. $Ho_2Mo_2O_{7-\delta}$ is a semiconductor with $\Delta \simeq 2000$ cm^{-1} (~0.25 eV) and $E_g \simeq 32\,000$ cm^{-1}. This is also indicated in the DC resistivity result shown earlier, but the value of the gap ($E_a \simeq 0.035$ eV) deduced from the DC resistivity is much smaller than that (Δ) from the AC conductivity. In $Gd_2Mo_2O_{7-\delta}$ E_g is reduced to $\simeq 27\,500$ cm^{-1} and, therefore, those two bands (Mo–O π^*a and R–O σ^* bands) overlap slightly. This leads to a band structure in which localized states separate from extended states by a mobility edge E_c. The Fermi energy E_F lies at the localized region 300–400 cm^{-1} below E_c, which has been estimated from both the optical and DC resistivity measurements in this paper, resulting in Anderson localization in this

crystal. It should be noted that Anderson localization can only happen where there exist some random potential fields to cause the localization of the one-electron wave function [9]. These fields could be built up by some oxygen deficiencies in the $Gd_2Mo_2O_{7-\delta}$ crystal. Recently, the oxygen content was determined by refinement of site occupation parameters on the x-ray data and δ turns out to be ~0.22 [23]. This can also be seen indirectly in the DC resistivity measurement on a fully oxygenated polycrystalline $Gd_2Mo_2O_{7-\delta}$ sample which exhibits a metallic behaviour [7]. $Sm_2Mo_2O_{7-\delta}$ is a metal because the full Mo–O π^*a band completely merges into the empty R–O σ^* band which can be seen from a further decrease of E_g to 25 000 cm^{-1}.

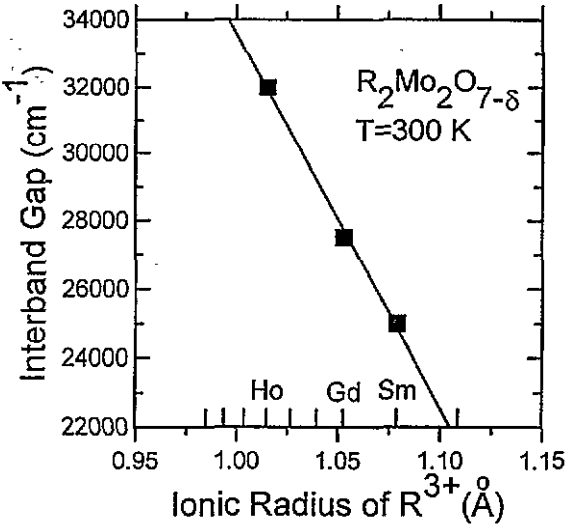

Figure 15. Interband gap of $R_2Mo_2O_{7-\delta}$ between the lower valence band and the conduction band as a function of the ionic radius of R^{3+} for the expected coordination. The solid straight line is the least-squares fit to the data.

4. Conclusions

The temperature dependences of the AC conductivity of the spin glass materials $Sm_2Mo_2O_{7-\delta}$, $Gd_2Mo_2O_{7-\delta}$, and $Ho_2Mo_2O_{7-\delta}$ were obtained by measuring the reflectance of these crystals and by performing Kramers–Kronig analysis on the resulting spectra. The conclusions that can be drawn are as follows.

(1) The AC conductivity of $Sm_2Mo_2O_{7-\delta}$ shows that it is a poor metal with a large Drude peak width at room temperature. With decreasing temperature it continues to exhibit a metallic behaviour. The scattering rate, which is deduced from fitting the far-infrared conductivity using the Drude formula, drops sharply between 150 and 40 K due to the scattering of the conduction electrons by short-range ordered moments of the Mo ions. The scattering rate saturates below 40 K because the moments are frozen in the spin glass state.

(2) The empty conduction band and the nearest full valence band overlap slightly in $Gd_2Mo_2O_{7-\delta}$ causing Anderson localization, in which the density of states at E_F is localized. At room temperature electrons are thermally excited to the mobility edge E_c and the AC conductivity is by optical excitations of those electrons in extended states. This results in a behaviour characteristic of a poor metal. In contrast, at low temperatures electrons

are localized and the low-frequency AC conductivity is achieved in terms of the optically activated hopping of electrons in localized states which shows a linear depression below 400 cm^{-1}. The localization of electronic states and the phonon-assisted hopping process cause the asymmetric shape of the phonon resonances in the conductivity spectra at low temperatures.

(3) $Ho_2Mo_2O_{7-\delta}$ is a semiconductor with a small gap of $\Delta \simeq 2000$ cm^{-1} (~0.25 eV). The gap value decreases a little as the temperature is reduced and does not change below 40 K. The far-infrared conductivity is independent of frequency at all temperatures. Its magnitude shifts downward between room temperature and 100 K and is independent of temperature below 100 K.

An interband transition peak was found in the ultraviolet region of all these crystals. The position of the peak increases linearly as the ionic radius of R^{3+} is decreased. It supports the following picture of a metal–semiconductor transition in $R_2Mo_2O_{7-\delta}$ within the SB model. The full narrow Mo–O π^*a valence band and the empty broad R–O σ^* conduction band are separated with a semiconducting gap for R = Ho in $Ho_2Mo_2O_{7-\delta}$. With the increase of the ionic radius for R = Gd these two bands overlap slightly due to the R–O σ^* band shifting downward and Anderson localization occurs for $Gd_2Mo_2O_{7-\delta}$. The degree of the overlap increases for R = Sm turning $Sm_2Mo_2O_{7-\delta}$ into a metal.

Acknowledgments

We would like to thank B D Gaulin, J P Carbotte, A J Berlinsky, and C Kallin for valuable discussions and R A Duncan and G Hewitson for technical support. This work was funded by the Natural Science and Engineering Research Council of Canada (NSERC).

References

[1] Reimers J N, Berlinsky A J and Shi A C, 1991 *Phys. Rev.* B **43** 865
[2] Gaulin B D, Reimers J N, Mason T E, Greedan J E and Tun Z 1992 *Phys. Rev. Lett.* **69** 3244
[3] Greedan J E, Sato M, Yan X and Razavi F S 1986 *Solid State Commun.* **59** 895
[4] Sato M, Yan X and Greedan J E, 1986 *Z. Anorg. (Allg.) Chem.* **540/541** 177
[5] Raju N P, Gmelin E and Kremer R K 1992 *Phys. Rev.* B **46** 5405
[6] Ford P J and Mydosh J A 1976 *Phys. Rev.* B **14** 2057
[7] Greedan J E, Sato M, Ali N and Datars W R 1987 *J. Solid State Chem.* **68** 300
[8] Sleight A W and Bouchard R J 1972 *Proc. 5th Materials Research Symp. (NBS special Publication 364)* p 227
[9] Anderson P W 1958 *Phys. Rev.* **109** 1492
[10] Reimers J N and Greedan J E 1988 *J. Solid State Chem.* 72 390
[11] Raju N P, Liu G, Cao N, Timusk T, Greedan J E and Gougeon P 1995 to be published
[12] Homes C C, Timusk T, Reedyk M and Crandles D A 1993 *Appl. Opt.* **32** 2976
[13] Fano U 1961 *Phys. Rev.* **124** 1866
[14] Barker A S Jr and Ditzenberger J A 1970 *Phys. Rev.* B **1** 4378
[15] Bonn D A, Garrett J D and Timusk T 1988 *Phys. Rev. Lett.* **61** 1305
[16] Cao N, Garrett J D and Timusk T 1993 *Physica* B **191** 263
[17] Mott N F and Davis E A 1971 *Electronic Processes in Non-crystalline Materials* (Oxford: Clarendon) p 51
[18] Jang H F, Gripps G and Timusk T 1990 *Phys. Rev.* B **41** 5152
[19] Mott N F 1974 *Metal-insulator Transitions* (London: Taylor and Francis) p 35, pp 46–47
[20] Raju N P and Rangarajan G 1990 *J. Phys.: Condens. Matter* **2** 3539
[21] Le Comber P G, Madan A and Spear W E 1972 *J. Non-Cryst. Solids* **11** 219
[22] Weber M J, Matsinger B H, Donlan V L and Surratt G T 1972 *J. Chem. Phys.* **57** 562
[23] Gougeon P, Raju N P, Liu Guo and Greedan J E 1995 to be published